JOURNAL OF THERMOPHYSICS AND HEAT TRANSFER
Vol. 10, No. 3, July–September 1996

Approximate Solution to Radiative Transfer in Two-Dimensional Cylindrical Media

Jose B. Pessoa-Filho* and Stefan T. Thynell†
Pennsylvania State University, University Park, Pennsylvania 16802

The development of an approximate solution to radiative transfer in two-dimensional, absorbing, emitting, scattering, cylindrical media is presented. The approach is based on an isolation of the discontinuities of the intensity prior to specifying the set of discrete ordinates. The discontinuities in the intensity or its slope at any point within the medium or at the bounding wall may be because of property variation along a bounding wall or at a corner, or the bounding geometry. The chosen set of discrete ordinates is based on Gaussian quadratures, and integrations are performed over solid angles over which the intensity is continuous and possesses continuous derivatives. Results for the incident radiation and radiative heat flux are presented for different physical configurations, and they are in good agreement with those available in the literature. In particular, approximately an order-of-magnitude fewer unknown intensities are involved in the solution to obtain results of accuracy comparable to the discrete-ordinates method.

Nomenclature

C	= height of the cylinder
c^*, c_1, c'	= interpolation coefficients
d	= distance
G	= incident radiation
I	= intensity of radiation
$\tilde{I}$	= interpolated intensity
I_b	= blackbody radiation intensity
i, j, k, l	= node location in the radial, axial, polar, and azimuthal directions, respectively
MR	= number of nodes in the r direction
MZ	= number of nodes in the z direction
q	= radiative heat flux
R	= radial dimension
r	= radial direction
S	= radiative source term
$\bar{S}$	= average radiative source term
s, s', s_0	= position variables
T	= temperature
z	= axial direction
β	= extinction coefficient
Δ	= difference
ε	= emissivity
θ	= polar angle
μ	= direction cosine
ξ	= weight of quadrature
ρ	= diffuse reflectivity
ϕ	= azimuthal angle
ω	= scattering albedo

Subscripts

b	= blackbody
$\hat{e}_r$	= unit vector in radial direction
$\hat{e}_z$	= unit vector in axial direction
m	= medium
1, 2, 3	= walls, 1, 2, 3

Superscripts

+	= positive values of μ
−	= negative values of μ
~	= interpolated quantity
-	= averaged quantity

Received May 1, 1995; revision received Nov. 29, 1995; accepted for publication Feb. 12, 1996.

*Graduate Student, Department of Mechanical Engineering.
†Associate Professor, Department of Mechanical Engineering. Member AIAA.

Introduction

THE study of radiative heat transfer in participating media has received a significant amount of attention during the past years because of its importance in many different areas including, among others, astrophysics, burning of liquid and solid propellants, fires, and the development of multilayer insulations for aerospace applications.[1] In many of these situations, the use of one-dimensional rather than multidimensional models for evaluating the radiation heat transfer may be questionable. Hence, new techniques for treating radiative heat transfer in multidimensional geometries have been presented in the literature.[2–8] Effects of multidimensionality, nongrayness, and spatially variable optical properties add mathematical and computational difficulties.[1] Unfortunately, in problems of practical interest, such as the ones involving radiative heat transfer in flames and furnaces, some of the effects just mentioned could be present. Additionally, it is usually necessary to solve the radiative heat transfer equation iteratively, since the temperature of the medium must be solved from an overall energy balance. Considering these aspects, the development of new methods of solution for solving the equation of radiative transfer accurately and computationally efficiently should be pursued.

The technique to be presented in this work is based on an isolation of the discontinuity in the radiation intensity. This technique has already been applied to one-dimensional geometries with excellent results.[9,10] The objective of this work is to show the applicability of the method for solving the equation of radiative transfer in two-dimensional cylindrical media.

Analysis

Physical Model

We consider radiative heat transfer in an emitting, absorbing, and isotropically scattering medium, as shown in Fig. 1. The radiative properties of the medium are gray and spatially varying. The walls emit and reflect the incident radiation diffusely. The temperature of the medium is assumed to be known from

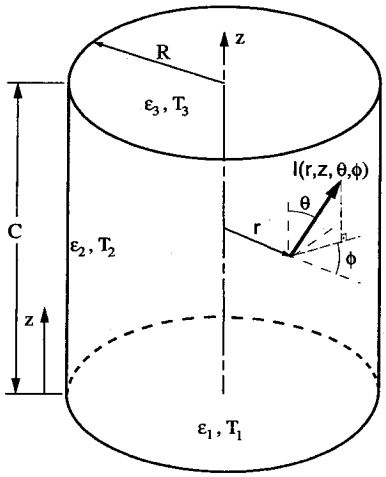

Fig. 1 Physical model and coordinates.

an overall energy balance. The equation of transfer to this problem can be written as[11]

$$\frac{1}{\beta(s)}\frac{dI(s)}{ds} + I(s) = S(s) \tag{1}$$

where

$$\frac{d}{ds} = \sin\theta\left(\cos\phi - \frac{\sin\phi}{r}\frac{\partial}{\partial\phi}\right) + \cos\theta\frac{\partial}{\partial z} \tag{2a}$$

$$S(s) = S(r, z) = [1 - \omega(r, z)]I_b[T_m(r, z)] + \frac{\omega(r, z)}{4\pi}\int_0^{2\pi}\int_0^{\pi} I(r, z, \theta, \phi)\sin\theta\, d\theta\, d\phi \tag{2b}$$

The boundary conditions for Eq. (1) are

$$I(r, 0, \theta, \phi) = \varepsilon_1 I_{b1}(r) + (\rho_1/\pi)q_{\hat{e}_z}^-(r, 0)$$
$$0 \le r < R, \quad 0 \le \theta < (\pi/2), \quad 0 \le \phi \le 2\pi \tag{3a}$$

$$I(R, z, \theta, \phi) = \varepsilon_2 I_{b2}(z) + (\rho_2/\pi)q_{\hat{e}_r}^+(R, z)$$
$$0 < z < C, \quad 0 < \theta < \pi, \quad (\pi/2) < \phi < (3\pi/2) \tag{3b}$$

$$I(r, C, \theta, \phi) = \varepsilon_3 I_{b3}(r) + (\rho_3/\pi)q_{\hat{e}_z}^+(r, C)$$
$$0 \le r < R, \quad (\pi/2) \le \theta < \pi, \quad 0 \le \phi \le 2\pi \tag{3c}$$

The incident radiation $G(r, z)$ and the forward and backward radiation heat fluxes in the r and z directions are, respectively, defined by

$$G(r, z) = 2\int_{\phi=0}^{\pi}\int_{\theta=0}^{\pi} I(r, z, \theta, \phi)\sin\theta\, d\theta\, d\phi \tag{4a}$$

$$q_{\hat{e}_r}^+(r, z) = 2\int_{\phi=0}^{\pi/2}\int_{\theta=0}^{\pi} I(r, z, \theta, \phi)\sin^2\theta\cos\phi\, d\theta\, d\phi \tag{4b}$$

$$q_{\hat{e}_z}^+(r, z) = 2\int_{\phi=0}^{\pi}\int_{\theta=0}^{\pi/2} I(r, z, \theta, \phi)\cos\theta\sin\theta\, d\theta\, d\phi \tag{4c}$$

$$q_{\hat{e}_r}^-(r, z) = 2\int_{\phi=0}^{\pi/2}\int_{\theta=0}^{\pi} I(r, z, \theta, \pi - \phi)\sin^2\theta\cos\phi\, d\theta\, d\phi \tag{4d}$$

$$q_{\hat{e}_z}^-(r, z) = 2\int_{\phi=0}^{\pi}\int_{\theta=0}^{\pi/2} I(r, z, \pi - \theta, \phi)\cos\theta\sin\theta\, d\theta\, d\phi \tag{4e}$$

An integration of Eq. (1) along path s over which the extinction coefficient is suitably averaged, $\beta(s) = \bar{\beta}$, yields[11]

$$I(s) = I(s_0)\exp[-\bar{\beta}(s - s_0)] + \bar{\beta}\int_{s_0}^{s} S(s')\exp[-\bar{\beta}(s - s')]\, ds' \tag{5}$$

Behavior of the Intensity

To acquire an insight into the discontinuous nature of the intensity, a purely absorbing medium bounded by black walls is considered. The medium and top surface are at zero temperature, i.e., $I_b[T_m(r, z)] = 0$ and $I_{b3}(r) = 0$, respectively. The temperatures of the bottom and peripheral walls are such that $I_{b1}(r) = 1.0$ and $I_{b2}(z) = 0.5$, respectively. Figure 2 illustrates the polar variation of the intensity ($\mu = \cos\theta$) at $r = 0$ and $z = C/2$. Examination of Fig. 2 reveals the existence of discontinuities at $\mu = \pm 0.5$. The qualitative behavior of the intensity distribution would be the same even if the medium contained scattering particles. In such a situation, the magnitude of the discontinuities decreases as the scattering albedo increases; however, discontinuities are still present. Note that the difficulty associated with the treatment of the discontinuity in the intensity field has been addressed previously.[12,13]

In developing an approximate method of solution to the equation of transfer, it is appropriate to consider the effects of discontinuities in the intensity. However, a wide variety of other aspects should also be considered.[1] They include, among others, nongray and spatially nonuniform properties, compatibility with solution techniques to the overall conservation of energy, momentum and species, as well as the effects of instabilities similar to those exhibited by the diamond discretization scheme of the discrete-ordinates method, if a set-to-zero or overshooting clipping is not used.[14,15]

Construction of Approximate Solution

The approximate solution to the radiative transfer equation to be developed considers the aspects mentioned previously. By assuming $S(s) = \bar{S}$, Eq. (5) can be written as

$$I(s) = I(s_0)\exp[-\bar{\beta}(s - s_0)] + \bar{S}(s)\{1 - \exp[-\bar{\beta}(s - s_0)]\} \tag{6}$$

where $\bar{S}$ and $\bar{\beta}$ represent, respectively, the average value of the source term and the extinction coefficient between s_0 and s. Note that the right-hand side (RHS) of Eq. (6) has only posi-

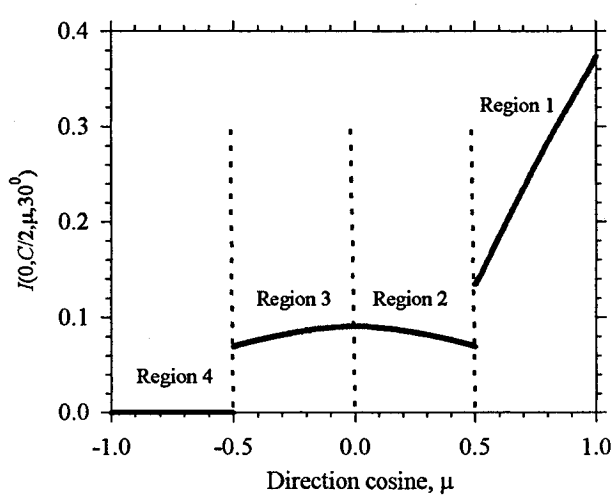

Fig. 2 Intensity distribution in the medium for $I_{b1}(r) = 1$, $I_{b2}(z) = 0.5$, $I_{b3}(r) = 0$, and $\omega = 0$. At $r = 0$ and $z = C/2$, the discontinuities are located at $\mu = \pm 0.5$.

tive terms and, as a consequence, instability problems have been eliminated.

The discontinuities in the intensity must be considered prior to an application of Eq. (6). The establishment of the angular positions where discontinuities occur is based on physical and geometrical considerations. For the case considered in Fig. 2, the intensity distribution in region 1 is governed by the one emanating from the bottom wall. In a similar fashion, the intensity distribution in region 4 is determined by the boundary condition applied to the top wall of the cylinder. Regions 2 and 3 have their intensity distribution determined by the boundary condition imposed by the peripheral wall. Although the intensity is a continuous function over regions 2 and 3, it is split into two separate regions to satisfy the limits of integration over the polar angle θ, given by Eqs. (4c) and (4e). The definition of the limits for each of the regions presented in Fig. 3 is based on geometrical considerations. For the ranges, $0 \leq \phi \leq 2\pi$, $0 \leq r < R$, and $0 < z < C$, the following regions are defined:

$$\text{Region 1: } \mu_0^+(r, z, \phi) < \mu \leq 1 \tag{7a}$$

$$\text{Region 2: } 0 < \mu < \mu_0^+(r, z, \phi) \tag{7b}$$

$$\text{Region 3: } \mu_0^-(r, z, \phi) < \mu \leq 0 \tag{7c}$$

$$\text{Region 4: } -1 \leq \mu < \mu_0^-(r, z, \phi) \tag{7d}$$

where

$$\mu_0^+(r, z, \phi) = \cos\left[\tan^{-1}\left(\frac{\sqrt{R^2 - r^2\sin^2\phi} + r\cos\phi}{z}\right)\right] \tag{8a}$$

$$\mu_0^-(r, z, \phi) = -\cos\left[\tan^{-1}\left(\frac{\sqrt{R^2 - r^2\sin^2\phi} + r\cos\phi}{C - z}\right)\right] \tag{8b}$$

At the bottom of the cylinder, the regions over which the intensity is continuous for $0 \leq \phi \leq 2\pi$ are given by

$$\text{Region 1: } 0 < \mu \leq 1 \tag{9a}$$

$$\text{Region 2: } \mu_0^-(r, 0, \phi) < \mu < 0 \tag{9b}$$

$$\text{Region 3: } -1 \leq \mu < \mu_0^-(r, 0, \phi) \tag{9c}$$

Similar equations can be derived for the top wall of the enclosure. Along the peripheral wall, the specification of angular positions for which the intensity is discontinuous is more complex. For $-\pi/2 < \phi < \pi/2$, the procedure employed previously for the inner regions of the medium is also used, and four regions over the polar angle are defined according to Eq. (7). Although the intensity is continuous along the inside of the peripheral wall, two regions are defined ($0 < \theta < \pi/2$ and $\pi/2 < \theta < \pi$) to satisfy the limits of integration imposed by Eqs. (4c) and (4e).

In heat transfer applications, calculations of the incident radiation and radiative heat flux are usually needed. To avoid repetition, the numerical integration procedure will be described only for the incident radiation. The integration is split over the azimuth angle to follow the limits of integration determined by Eqs. (4b) and (4d), and because of symmetry, only half of its angular span needs to be considered. Thus, Eq. (4a) becomes

$$G(r, z) = 2\int_{\phi=0}^{\pi/2}\int_{-1}^{1} I(r, z, \mu, \phi)\, d\mu\, d\phi + 2\int_{\phi=\pi/2}^{\pi}\int_{-1}^{1} I(r, z, \mu, \phi)\, d\mu\, d\phi \tag{10}$$

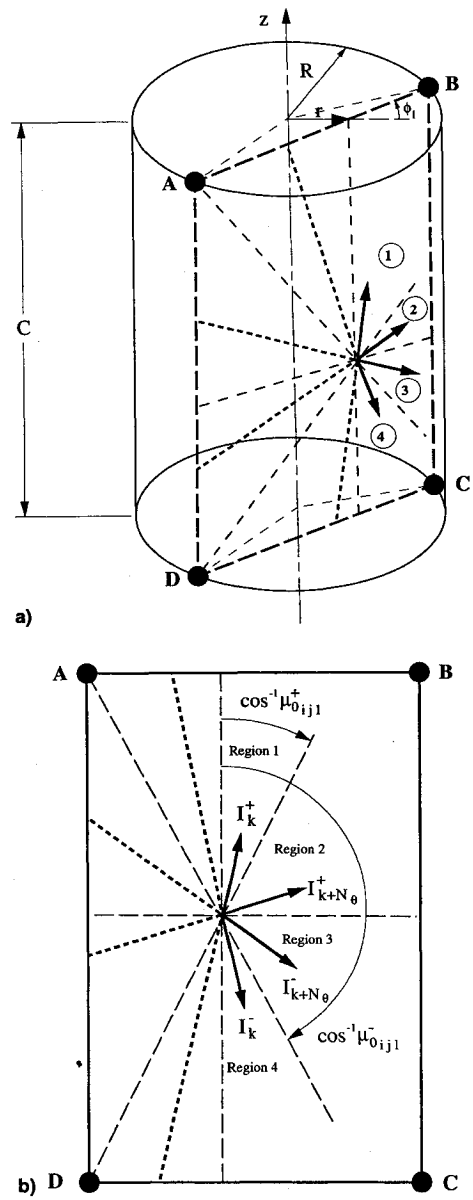

Fig. 3 a) Geometrical configuration illustrates the division of the θ domain into four regions and b) plane ABCD shows the angular limit of each region and the relative position of $I^{\pm}_{ijkl}$, $k = 1, \ldots, 2N_\theta$.

The evaluation of the integral over the polar angle is split into four different regions, as defined by Eqs. (7), namely

$$\int_{-1}^{1} I(r, z, \mu, \phi)\, d\mu = \int_{-1}^{\mu_0^-(r,z,\phi)} I(r, z, \mu, \phi)\, d\mu + \int_{\mu_0^-(r,z,\phi)}^{0} I(r, z, \mu, \phi)\, d\mu + \int_{0}^{\mu_0^+(r,z,\phi)} I(r, z, \mu, \phi)\, d\mu + \int_{\mu_0^+(r,z,\phi)}^{1} I(r, z, \mu, \phi)\, d\mu \tag{11}$$

A quadrature formula is now applied to evaluate each one of the integrals in Eq. (11). The following notation is used:

$$I^{\pm}_{ijkl} = I^{\pm}(r_i, z_j, \mu_k, \phi_l) \tag{12a}$$

$$\mu^{\pm}_{0ijl} = \mu^{\pm}_0(r_i, z_j, \phi_l) \tag{12b}$$

Figure 3b schematically shows the various directions of the intensity in the plane ABCD of Fig. 3a. The indices referring to the r, z, and ϕ coordinates are omitted to avoid overcrowding. By applying the quadrature to Eq. (11), we obtain

$$P_{ijl} = \int_{-1}^{1} I(r, z, \mu, \phi_l)\, d\mu \simeq \frac{1}{2}\sum_{k=1}^{N_\theta} \xi_k[(1 + \mu_{0ijl})I^-_{ijkl} - \mu^-_{0ijl}I^-_{ijk+N_\theta l} + \mu^+_{0ijl}I^+_{ijk+N_\theta l} + (1 - \mu^+_{0ijl})I^+_{ijkl}] \quad (13)$$

Applying a quadrature to perform the integration over all azimuth angles, and using the notation defined by Eq. (13), Eq. (10) becomes

$$G(r, z) \simeq G_{ij} = \frac{\pi}{2}\sum_{l=1}^{N_\phi} \xi_l(P_{ijl} + P_{ijl+N_\phi}) \quad (14)$$

The numerical integration of Eq. (10) can be summarized as follows: the polar angle is split into four different regions defined by Eqs. (7), whereas the azimuth angle is split into two regions: $0 < \phi < \pi/2$ and $\pi/2 < \phi < \pi$. A quadrature is applied to each region of the polar and azimuth angles. After obtaining P_{ijl}, $l = 1, \ldots, 2N_\phi$, Eq. (14) is used to evaluate $G(r, z)$. The procedures employed along the bottom and top walls are similar except that only three regions are defined by Eqs. (9). Along the peripheral walls, Eq. (11) is valid for $0 < \phi < \pi/2$; for $\pi/2 < \phi < \pi$, the intensity is continuous over the polar angle. However, to satisfy the limits imposed by Eqs. (4c) and (4e), one region is defined for $0 < \theta < \pi/2$ and another for $\pi/2 < \theta < \pi$.

Form of Approximate Solution

By using the notation defined by Eqs. (12), Eq. (6) can be approximated as

$$I^{\pm}_{ijkl} = \tilde{I}^{\pm}_{ijkl} \exp[-(\bar{\beta}\Delta s)^{\pm}_{ijkl}] + \bar{S}^{\pm}_{ijkl}\{1 - \exp[-(\bar{\beta}\Delta s)^{\pm}_{ijkl}]\} \quad (15)$$

The procedure for evaluating the various terms in Eq. (15) is involved. For a particular problem, many configurations may occur producing lengthy derivations for the expressions of $\tilde{I}^{\pm}_{ijkl}$, $\Delta s^{\pm}_{ijkl}$, $\bar{\beta}^{\pm}_{ijkl}$, and $\bar{S}^{\pm}_{ijkl}$. Therefore, derivation of the equations is presented only for a frequently found configuration to outline the general procedure behind the technique. Initially, the physical domain in the r and z directions is evenly discretized according to

$$\Delta r = R/(MR - 1) \quad (16a)$$

$$\Delta z = C/(MZ - 1) \quad (16b)$$

To avoid the discontinuity of the intensity at the corner of the cylinder, no node is defined at $(R, 0)$ and (R, C) locations. To illustrate the calculational procedure of $\tilde{I}^{\pm}_{ijkl}$, $\Delta s^{\pm}_{ijkl}$, $\bar{\beta}^{\pm}_{ijkl}$, and $\bar{S}^{\pm}_{ijkl}$, the configuration represented schematically in Fig. 4 is considered. In this case, the evaluation of $\tilde{I}^{+}_{ijkl}$ at node (i, j) is desired. From geometrical considerations

$$\Delta s^{+}_{ijkl} = \Delta d_{jl}/\sqrt{1 - \mu^{+2}_{ijkl}} \quad (17)$$

where Δd_{jl} is illustrated in Fig. 5. Three configurations are possible:

$$1:\ \Delta d_{il} = r_i \cos\phi_l - \sqrt{r^2_{i-1} - r^2_i \sin^2\phi_l},\quad 0 < \phi < \psi_i \quad (18a)$$

$$2:\ \Delta d_{il} = 2r_i \cos\phi_l,\quad \psi_i < \phi < \pi/2 \quad (18b)$$

$$3:\ \Delta d_{il} = r_i \cos\phi_l + \sqrt{r^2_{i+1} - r^2_i \sin^2\phi_l},\quad \pi/2 < \phi < \pi \quad (18c)$$

$$\psi_i = \cos^{-1}[\sqrt{1 - (r_{i-1}/r_i)^2}] \quad (18d)$$

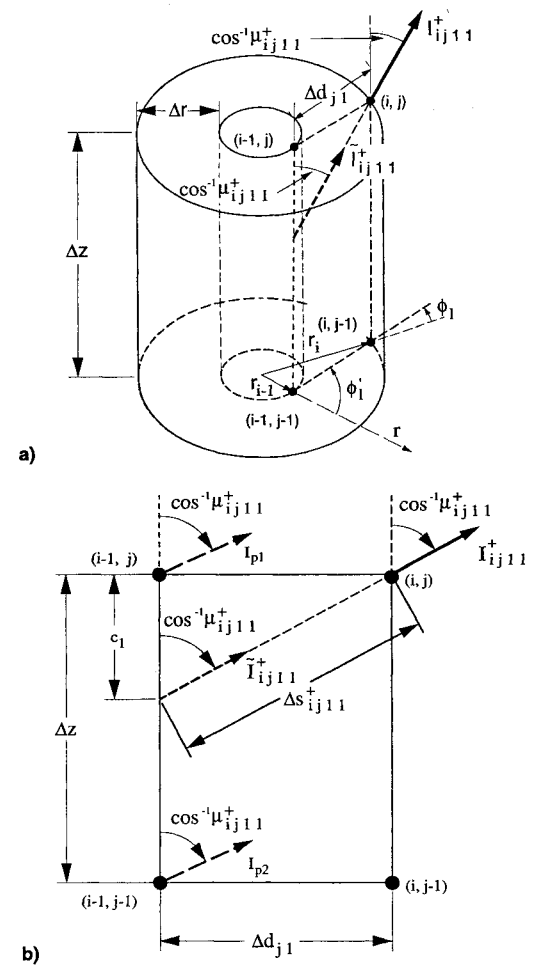

Fig. 4 a) Location of $\tilde{I}^{+}_{i,j,1,1}$ relative to $I^{+}_{i,j,1,1}$ and b) $\tilde{I}^{+}_{i,j,1,1}$ is evaluated from a linear interpolation using I_{p1} and I_{p2}.

The calculation of $\tilde{I}^{+}_{ijkl}$ is more involved because it is located at a point in space where no node is defined, as shown in Fig. 4a. Therefore, its value is approximated from an interpolation using the intensities at nodes $(i - 1, j)$ and $(i - 1, j - 1)$, shown in Fig. 4b. In addition, the direction of $\tilde{I}^{+}_{ijkl}$ is determined by the values of μ^{+}_{ijkl} and ϕ_l. Since values of μ_k at nodes $(i - 1, j)$ and $(i - 1, j - 1)$, are different from values of μ_k at node (i, j), interpolation over the polar angle is necessary at both nodes. Furthermore, because of curvature effects, ϕ_l is different from ϕ'_l, as shown in Fig. 4a. As a result, interpolation is also necessary over the azimuth angle.

In Fig. 4b, I_{p1} and I_{p2} represent interpolated values of intensities, in the μ^{+}_{ijkl} and ϕ'_l directions, at nodes $(i - 1, j)$ and $(i - 1, j - 1)$, respectively. The calculation procedure for I_{p1} is presented. Without loss of generality, let us assume $N_\phi = 2$, $N_\theta = 2$, $k = 1$, and $l = 1$. Figure 6a illustrates a top view of node $(i - 1, j)$, showing the three ϕ angles considered. Assuming $\phi_1 < \phi'_1 < \phi_2$, interpolations are required over both azimuth angles ϕ_1 and ϕ_2 to calculate the intensities in direction of μ^{+}_{ij11}. To avoid overcrowding, the indices corresponding to the radial and axial directions are not shown in Fig. 6b. $\bar{I}_1$ represents the interpolated intensity in the ϕ_1 direction, over angle μ^{+}_{ij11}. If linear interpolation is used, $\bar{I}_1$ is given by

$$\bar{I}_1 = c^* I^{+}_{i-1j11} + (1 - c^*) I^{+}_{i-1j21} \quad (19a)$$

where

$$c^* = \frac{\mu^{+}_{ij11} - \mu^{+}_{i-1j21}}{\mu^{+}_{i-1j11} - \mu^{+}_{i-1j21}} \quad (19b)$$

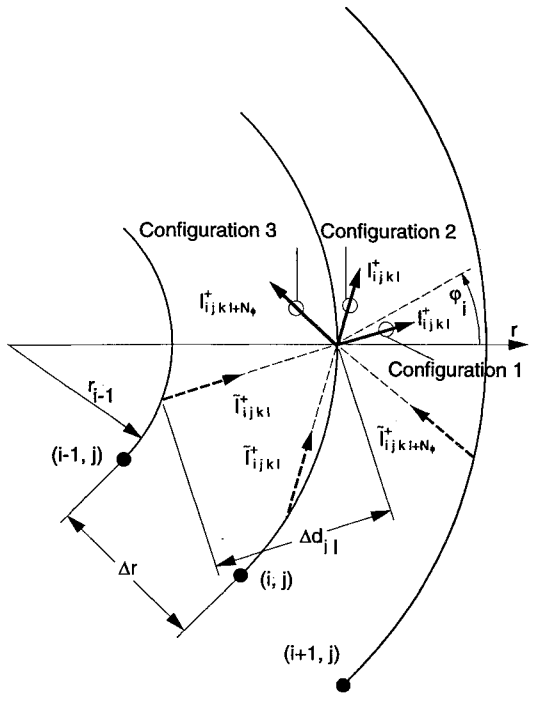

Fig. 5 Three configurations are possible in determining the location of $\tilde{I}^{+}_{ijkl}$ in the ϕ direction.

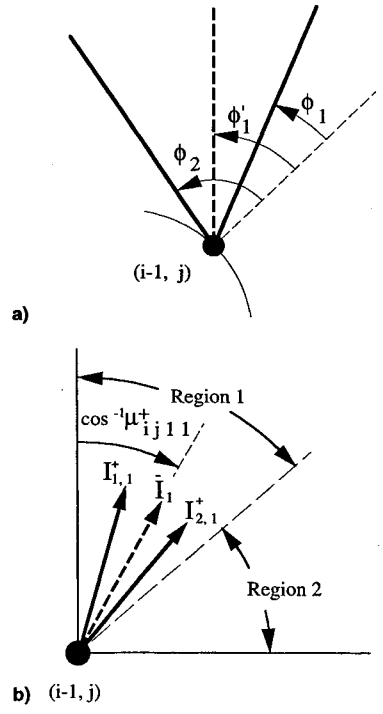

a)

b)

Fig. 6 a) Top view of node $(i-1, j)$ showing the relative position of ϕ_1' with respect to ϕ_1 and ϕ_2 and b) representation of intensities in direction of ϕ_1.

$\bar{I}_2$, in the ϕ_2 direction, is obtained in a similar fashion. I_{p1} is obtained from linear interpolation between $\bar{I}_1$ and $\bar{I}_2$, namely

$$I_{p1} = c'\bar{I}_2 + (1 - c')\bar{I}_1 \tag{20a}$$

where

$$c' = (\phi_1' - \phi_1)/(\phi_2 - \phi_1) \tag{20b}$$

A similar procedure is carried out at node $(i-1, j-1)$ to determine I_{p2}. Once I_{p1} and I_{p2} have been determined, the final interpolation is carried out to yield $\tilde{I}^{+}_{ij11}$. We have

$$\tilde{I}^{+}_{ij11} = (c_1/\Delta z)I_{p2} + [1 - (c_1/\Delta z)]I_{p1} \tag{21a}$$

$$c_1 = \Delta s^{+}_{ij11}\mu^{+}_{ij11} \tag{21b}$$

A total of seven interpolations is performed to calculate $\tilde{I}^{+}_{ij11}$. The coefficients used in the interpolation procedure are dependent on the geometrical configuration and the number of nodes in the r, z, θ, and ϕ directions. Therefore, they are calculated and stored at the beginning of the iterative procedure. The calculations of $\bar{S}^{+}_{ij11}$ and $\bar{\beta}^{+}_{ij11}$ are made by taking the average value of $S(s)$ and $\beta(s)$, respectively, between $\tilde{I}^{+}_{ij11}$ and I^{+}_{ij11}. Hence,

$$\bar{S}^{+}_{ij11} = 0.5(\{(c_1/\Delta z)S_{i-1j-1} + [1 - (c_1/\Delta z)]S_{i-1j}\} + S_{ij}) \tag{22a}$$

$$\bar{\beta}^{+}_{ij11} = 0.5(\{(c_1/\Delta z)\beta_{i-1j-1} + [1 - (c_1/\Delta z)]\beta_{i-1j}\} + \beta_{ij}) \tag{22b}$$

The terms in braces in Eqs. (22) represent the evaluation of $S(s)$ and $\beta(s)$ at the location where $\tilde{I}^{+}_{ij11}$ is calculated. Nevertheless, the most important aspect of the interpolation procedure is that interpolated intensities must belong to the same angular region as the intensity to be determined. In the previous case, it is necessary to ensure that all intensities used at nodes $(i-1, j)$ and $(i-1, j-1)$ belong to region 1. Mathematically, this condition is defined as

$$\mu^{+}_{0i-1,j,1} < \mu^{+}_{ij11} < 1 \tag{23a}$$

$$\mu^{+}_{0i-1,j,2} < \mu^{+}_{ij11} < 1 \tag{23b}$$

$$\mu^{+}_{0i-1,j-1,1} < \mu^{+}_{ij11} < 1 \tag{23c}$$

$$\mu^{+}_{0i-1,j-1,2} < \mu^{+}_{ij11} < 1 \tag{23d}$$

The conditions represented by Eqs. (23) come from two fundamental aspects of the problem. First, since the intensity is discontinuous in the μ direction, it is mathematically incorrect to use intensities from two different regions to calculate either $\bar{I}_1$ or $\bar{I}_2$. For example, if the interpolation to obtain $\bar{I}_1$ in Fig. 6b involved one intensity from region 1 and another from region 2, the interpolation procedure would be incorrect. The interpolation would have been carried out over an interval in which the intensity is discontinuous. Second, referring to the purely absorbing medium bounded by black walls, it is known that the boundary condition at the peripheral wall of the cylinder does not have any effect on the intensity distribution in region 1. Therefore, if intensities from region 2 are used to obtain either $\bar{I}_1$ or $\bar{I}_2$, information from the peripheral wall is incorrectly transmitted to region 1, leading to a physically unrealistic calculation. This kind of error is introduced into the classical discrete-ordinates method, as a result of the method of discretization (either step or diamond schemes). It is usually referred to as false scattering, because the mechanism responsible for the change in direction of the beam of radiation is not physical but numerical.[14,15]

If one or more of the conditions specified by Eqs. (23) are not verified, the interpolation moves to another region. The general rule here is that one moves backwards along the line defined by (i, j), μ^{+}_{ijkl} and ϕ_l, until any horizontal or vertical line joining two nodes is intersected. Once such a line is found, the conditions of continuity of the intensity are verified for each one of the nodes and directions from which $\bar{I}_1$ and $\bar{I}_2$ are to be calculated. If these conditions are not verified, one continues to move backwards until another horizontal or vertical line that obeys the continuity condition is found.

The configuration shown in Fig. 4 is among those most frequently found when calculating intensities within the medium.

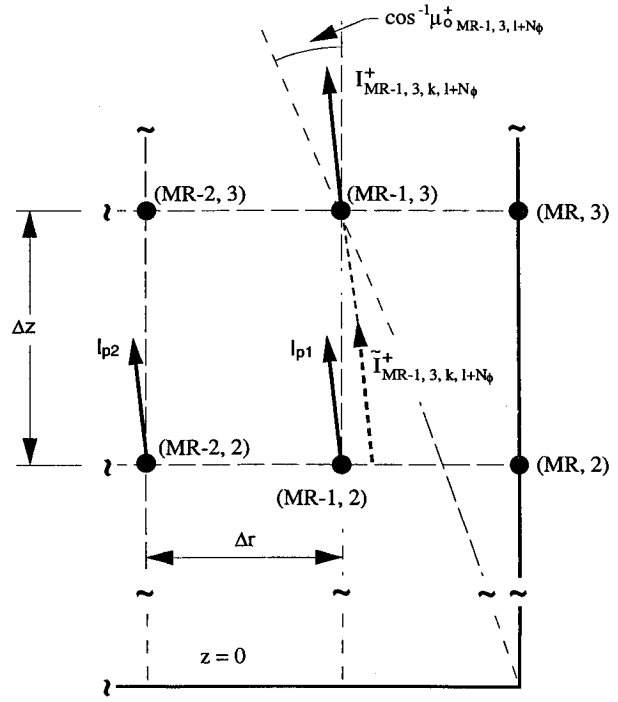

Fig. 7 Schematic representation of extrapolation procedure that takes place close to the boundaries. $\tilde{I}^{+}_{MR-1,3,k,l+N_\phi}$ is obtained from linear extrapolation using I_{p1} and I_{p2}.

However, to further clarify the technique, a configuration that appears close to the boundary is considered: calculation of $I^{+}_{MR-1,3,k,l+N_\phi}$, $k \leq N_\theta$, at node $(MR-1, 3)$ as shown in Fig. 7. Since $I^{+}_{MR-1,3,k,l+N_\phi}$ belongs to region 1, $\tilde{I}_1$ and $\tilde{I}_2$ must be calculated by using intensities in region 1. For the configuration shown in Fig. 7, the use of node $(MR, 2)$ is not allowed since, by definition, only regions 2 and 3 are defined at the peripheral inner wall of the cylinder. In this case, $\tilde{I}^{+}_{MR-1,3,k,l+N_\phi}$, $\bar{S}^{+}_{MR-1,3,k,l+N_\phi}$, and $\bar{\beta}^{+}_{MR-1,3,k,l+N_\phi}$ are calculated from extrapolation at nodes $(MR-1, 2)$ and $(MR-2, 2)$ using

$$\tilde{I}^{+}_{MR-1,3,k,l+N_\phi} = -(c_1/\Delta r)I_{p2} + [1 + (c_1/\Delta r)]I_{p1} \quad (24a)$$

$$\bar{S}^{+}_{MR-1,3,k,l+N_\phi} = 0.5(\{-(c_1/\Delta r)S_{MR-2,2} + [1 + (c_1/\Delta r)]S_{MR-1,2}\} + S_{MR-1,3}) \quad (24b)$$

$$\bar{\beta}^{+}_{MR-1,3,k,l+N_\phi} = 0.5(\{-(c_1/\Delta r)\beta_{MR-2,2} + [1 + (c_1/\Delta r)]\beta_{MR-1,2}\} + \beta_{MR-1,3}) \quad (24c)$$

$$c_1 = \Delta s^{+}_{MR-1,3,k,l+N_\phi}\sqrt{1 - (\mu^{+}_{MR-1,3,k,l+N_\phi})^2} \quad (24d)$$

Numerical Procedure

In this work, Gauss–Legendre[16] quadratures were used. Except for the boundary conditions, given by Eqs. (3), all intensities were initially set equal to zero. The iterative procedure was started by calculating all geometrical parameters, followed by the calculation of $I^{\pm}_{ijkl}$ using Eq. (15). I^{+}_{ijkl} and $I^{-}_{MZ-i+1,j,k,l}$ were calculated simultaneously to use symmetry in the geometrical parameters and to accelerate the convergence. The calculation of I^{+}_{ijkl} started at $i = 2$ and moved towards $MZ - 1$, $j = MR - 1, \ldots, 1$. At each node (i, j), $k = 1, \ldots, 2N_\theta$, whereas $l = 1, \ldots, 2N_\phi$. Therefore, for each node within the medium, $I^{\pm}_{ijkl}$ was calculated in $8N_\theta N_\phi$ directions. At the top and bottom walls of the cylinder, $I^{\pm}_{ijkl}$ was calculated in $6N_\theta N_\phi$ different directions, since only three regions are defined. The following convergence criterion was applied:

$$\frac{|G^{(n+1)}_{ij} - G^{(n)}_{ij}|}{G^{(n+1)}_{ij}} \leq 10^{-5} \quad (25)$$

where the superscript $(n + 1)$ denotes results from the last iterative step. To obtain the results shown in the next section, a computational algorithm was developed and implemented on a DEC 300–400 computer.

Discussion of Results

Since the calculation of the intensity requires a total of seven interpolations and, in some situations extrapolations, it is important to access their effects on the accuracy of the results. With this purpose, we consider a nonemitting, nonscattering medium ($\omega = 0$) bounded by black walls. The optical dimensions of the medium are $\beta R = 0.5$ and $\beta C = 1$. The top wall is at zero temperature, whereas the bottom and peripheral walls are at different temperatures, such that $I_{b1}(r) = 0.5$, $I_{b2}(z) = 1$. Since $\beta(s) = 1$ and $S(s) = 0$, Eq. (15) becomes

$$I^{\pm}_{ijkl} = \tilde{I}^{\pm}_{ijkl} \exp(-\Delta s^{\pm}_{ijkl}) \quad (26)$$

Considering that $\Delta s^{\pm}_{ijkl}$ is obtained in an exact fashion, the accuracy of the obtained results for the intensity is dependent on how accurately $\tilde{I}^{\pm}_{ijkl}$ is evaluated. Six combinations of (MR, MZ) and four combinations of (N_θ, N_ϕ) are used in this investigation. Table 1 shows the obtained results for the intensity at $r = R$, $z = C/2$. For each set (N_θ, N_ϕ), the column on the left represents an intensity located in region 1 of Fig. 3, while the column on the right represents an intensity in region 2. No results are presented for region 3 because they are the same as those of region 2 because of symmetry. The intensity within region 4 is equal to zero.

Inspection of Table 1 reveals that for any combination (N_θ, N_ϕ), the presented results are in excellent agreement with those obtained from the exact solution of the equation of radiative transfer, which is readily obtained in the nonscattering case.[11] Also note that MR, MZ, N_θ, and N_ϕ can be independently varied without changing the obtained results significantly. In general, by keeping (N_θ, N_ϕ) constant and increasing (MR, MZ), there is a decrease in the accuracy of the solution. Since $\beta(s) = 1$ and $S(s) = 0$, the increase in (MR, MZ) does not change the evaluation of $\bar{\beta}$ and $\bar{S}$, but it significantly increases the number of extrapolations, resulting in a slight increase in the

Table 1 Effects of number of spatial nodes and discrete ordinates on the convergence of the intensity with $r = R$, $z = C/2$, and different values of θ and ϕ: $I_{b1}(r) = 0.5$, $I_{b2}(z) = 1$, $I_{b3}(r) = 0$, $I_b[T_m(r, z)] = 0$, $\omega = 0$

	a			
	$N_\theta = 2, N_\phi = 2$		$N_\theta = 2, N_\phi = 3$	
MR, MZ	$\theta = 54$ deg, $\phi = 19$ deg	$\theta = 84$ deg, $\phi = 19$ deg	$\theta = 48$ deg, $\phi = 45$ deg	$\theta = 83$ deg, $\phi = 45$ deg
5, 7	0.21028	0.38559	0.23618	0.49215
5, 11	0.20818	0.38565	0.23546	0.49726
11, 11	0.21188	0.38603	0.23458	0.48730
11, 21	0.20717	0.38626	0.23370	0.48727
21, 21	0.20871	0.38630	0.23372	0.48578
41, 41	0.20685	0.38465	0.23305	0.48329
Exact	0.21116	0.38672	0.23618	0.49046
	b			
	$N_\theta = 3, N_\phi = 3$		$N_\theta = 5, N_\phi = 5$	
	$\theta = 38$ deg, $\phi = 45$ deg	$\theta = 73$ deg, $\phi = 45$ deg	$\theta = 38$ deg, $\phi = 45$ deg	$\theta = 73$ deg, $\phi = 45$ deg
5, 7	0.26471	0.47945	0.26461	0.47904
5, 11	0.26374	0.48873	0.26415	0.48783
11, 11	0.26423	0.47392	0.26534	0.47733
11, 21	0.26304	0.47300	0.26341	0.47809
21, 21	0.26330	0.47103	0.26369	0.47564
41, 41	0.26278	0.46696	0.26301	0.47131
Exact	0.26524	0.47781	0.26524	0.47781

error of the solution. If nodes were defined at the boundaries only, $\tilde{I}^{\pm}_{ijkl}$ would be evaluated in an exact fashion and Eq. (26) would yield exact values of $I^{\pm}_{ijkl}$. As MR and MZ increase, more extrapolations are carried out resulting in a decrease of the accuracy of the obtained results. From the results presented in Table 1, however, it is clear that the interpolation and extrapolation procedures used in this technique do not lead to large errors in the obtained solution even for large values of MR, MZ, N_θ, and N_ϕ.

It is also observed from Table 1, that for a fixed value of (MR, MZ) an increase in (N_θ, N_ϕ) causes an improvement in the accuracy of the solution. Such a comparison is possible for (N_θ, N_ϕ) corresponding to (3, 3) and (5, 5) in Table 1b, since the intensities are represented at the same spatial locations and directions. Such a result is expected since the use of more nodes in the θ and ϕ directions tends to more accurately describe the intensity distribution. The case corresponding to $N_\theta = N_\phi = 2$, $MR = 5$, and $MZ = 7$ took about 0.3 CPU seconds using a DEC 300–400 computer, whereas the case corresponding to $N_\theta = N_\phi = 5$, $MR = MZ = 41$ took about 740 CPU seconds.

The second case considers a nonscattering medium bounded by gray walls. As in the previous case, the objective is to evaluate the accuracy of the method when discontinuities in the intensity are more severe ($\omega = 0$). Here, again, the intensity of radiation is given by Eq. (26) and, consequently, the accuracy of the solution is strongly dependent on the accurate evaluation of $\tilde{I}^{\pm}_{ijk}$. The medium, top, and peripheral walls of the cylinder are at zero temperature, i.e., $I_b[T_m(r, z)] = 0$, $I_{b3}(r) = 0$, $I_{b2}(z) = 0$, respectively. The bottom wall is at uniform temperature $I_{b1}(r) = 1$. The walls are assumed to be gray with $\varepsilon_i = 0.5$, $i = 1, 2, 3$, $\beta C = 1$, and $\beta R = 0.5$. Results are presented for the radiosities at the walls of the cylinder, i.e., $J_1(r)$, $J_2(z)$, and $J_3(r)$, defined by the RHS of Eqs. (3a–3c), respectively. Six radial nodes and nine axial nodes were used with $N_\theta = N_\phi = 2$. The obtained results for the radiosities at the walls are shown in Table 2. For comparison purposes, the results obtained by Thynell[6] are also included in Table 2. The results for $J_1(r)$ and $J_3(r)$ are within 0.5% relative error compared with those obtained by Thynell.[6]

The results obtained for $J_2(z)$ are in good agreement with those computed by Thynell,[6] but are not as accurate as the ones obtained for $J_1(r)$ and $J_3(r)$. Inspection of Table 2 reveals that the largest relative error occurs at the first node along the peripheral wall (MR, 1). At this location, the relative error is about 4%. Such a result suggests that the inaccuracy is caused by some of the approximations introduced by this technique. The calculation of intensities within region 2, at nodes located at (MR, 1) and (i, 2), $i = 1, \ldots, MR$, involves extrapolation of the intensities located at nodes ($i - 1$, 2) and ($i - 1$, 3), $i = 2, \ldots, MR$, in a similar way as shown in Fig. 7. Because of the boundary conditions, the intensity at node ($MR - 1$, 2) is larger than the intensity at node ($MR - 1$, 3). Furthermore, to avoid the discontinuity at the corner, the node (MR, 1) is located at $z/C = 0.01$. As a result, the extrapolation to obtain $\tilde{I}^{+}_{MR,1,k,l}$ overestimates the value of $I^{+}_{MR,1,k,l}$. An increase in the number of nodes improves the accuracy, but extrapolations are still needed at nodes close to the bottom wall.

The numerical integration scheme also affects the results along the peripheral wall of the cylinder. The evaluation of $q_{e_z}(r, z)$ involves μ in the integrand, whereas $q_{e_r}(r, z)$ involves the highly nonlinear term $(1 - \mu^2)^{1/2}$. As a result, the values obtained for $q_{e_z}(r, z)$ are more accurate than those obtained for $q_{e_r}(r, z)$. Since $J_2(z)$ is dependent on $q^{+}_{e_r}(R, z)$, whereas $J_1(r)$ and $J_3(r)$ are dependent on $q^{\pm}_{e_z}(r, z)$, the obtained results for $J_2(z)$ are less accurate.

The next problem considers a purely scattering medium ($\omega = 1$). The walls of the cylinder are black. The bottom and top walls are at zero temperature, whereas the peripheral wall is at high temperature, $I_{b2} = 1$. Here, $\beta R = 1$ and $\beta C = 2$, $N_\theta = N_\phi = 2$ and an evenly spaced grid with $MR = 10$ and $MZ = 21$ are used. Results for the net heat flux at the bottom $-q_{e_z}(r, 0)$, and peripheral $-q_{e_r}(R, z)$, walls of the cylinder are shown in Fig. 8. Jendoubi et al.[7] investigated this problem using the $S - 14$ discrete-ordinates method.

A comparison between the results obtained in this work and those obtained by Jendoubi et al.[7] for the net radiative heat flux at the bottom and peripheral walls reveals that the two sets of results agree exceptionally well. Reference 21 of Jendoubi et al.[7] indicates that 25 nodes were used in both r and z directions. Since they used the $S - 14$ discrete-ordinates method, a total of 112 intensities was evaluated at each node, per iteration. Therefore, at each iteration, 70,000 unknowns were calculated. By applying the technique presented in this work and calculating the intensity in 32 directions ($N_\theta = N_\phi = 2$) and 210 nodes ($MR = 10$ and $MZ = 21$), it was possible to obtain results with the same level of accuracy as the $S - 14$ discrete-ordinates method. It should be mentioned, however, that Ref. 21 of Jendoubi et al.[7] indicates that the use of the $S - 8$ discrete-ordinates method gives the same level of accuracy as the $S - 14$ discrete-ordinates method. Nonetheless, it does not elaborate on the spatial resolution. It is also shown in Ref. 21 of Jendoubi et al.[7] that the results by the discrete-ordinates method are strongly dependent on the discretization scheme (e.g., positive, diamond, and step schemes). For example, results obtained by the diamond scheme for the incident radiation at the midplane of the cylinder were physically unrealistic, whereas the ones obtained by the use of either diamond or positive scheme exhibited oscillations in the incident radiation distribution along the radial direction.

Table 2 Radiosities at the bottom, top, and peripheral walls of a nonemitting and nonscattering medium bounded by gray walls, $\varepsilon_i = 0.5$, $i = 1, 2, 3$; $I_{b1}(r) = 1$, $I_{b2}(z) = 0$, $I_{b3}(r) = 0$

Radiosity at the bottom wall, $J_1(r)$					
r/R	0	0.25	0.50	0.75	0.98
This work	1.6039	1.6063	1.6137	1.6336	1.6891
Thynell[6]	1.6013	1.6032	1.6098	1.6242	1.6782
Radiosity at the top wall, $J_3(r)$					
r/R	0	0.25	0.50	0.75	0.98
This work	0.0741	0.0728	0.0688	0.0625	0.0557
Thynell[6]	0.0742	0.0727	0.0686	0.0624	0.0559
Radiosity at the peripheral wall, $J_2(z)$					
z/C	0.01	0.25	0.50	0.75	0.99
This work	0.4276	0.1771	0.0887	0.0512	0.0376
Thynell[6]	0.4094	0.1746	0.0875	0.0491	0.0357

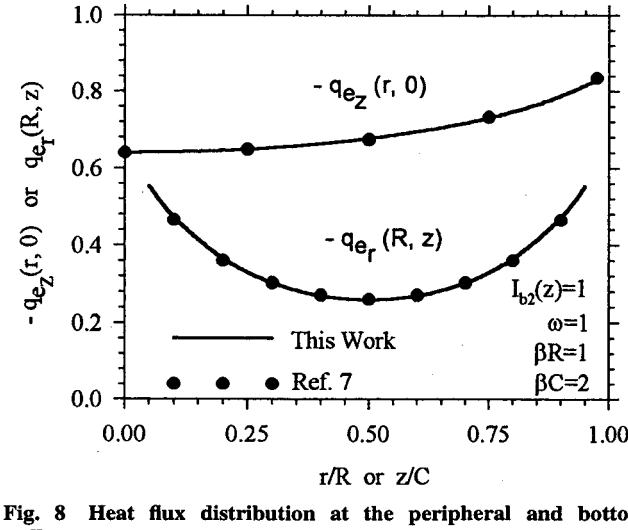

Fig. 8 Heat flux distribution at the peripheral and bottom walls.

Summary and Conclusions

The development of an approximate method of solution has been presented for solving the equation of radiative transfer in two-dimensional cylindrical geometry. The technique is based on the isolation of the discontinuities of the intensity. Results for the net heat flux and incident radiation are obtained for different geometrical configurations. The obtained results are compared with other results available in the literature and good agreement is observed. A comparison with the classical discrete-ordinates method suggests that the technique developed in this work is capable of giving the same level of accuracy as the discrete-ordinates method, but involving fewer unknown intensities. Because of the mathematical form of the solution, fix-up procedures such as set-to-zero and overshooting clipping of the intensity were not necessary. Moreover, no oscillatory behavior was observed in any of the solutions.

Also note that most of the results presented in the literature are for highly scattering media. In such cases, effects of false scattering are less evident than for situations involving nonscattering media. In nonscattering media, the effects of discontinuities in the intensity are more pronounced.

Finally, it should be mentioned that implementation of the technique to multidimensional geometries may be cumbersome because of the necessity of deriving and programming many different geometrical configurations and interpolation procedures. An increase on the complexity of the geometry adds more difficulties to the implementation of the technique. In view of the accurate results obtained, the additional effort in programming and deriving the different configurations is compensated by the significant decrease in the computational effort. This is important in problems involving nongray gases and when radiative transfer is coupled to conduction and convection. In these situations, the equation of transfer is solved repeatedly and, the computational time is an important aspect to consider.

Acknowledgments

This work was partially performed under Contracts DAAL03-92-G-0020 and DAAH04-95-1-0268 with D. M. Mann, U.S. Army Research Office, Research Triangle Park, North Carolina, serving as the Program Manager.

References

[1]Howell, J. R., "Thermal Radiation in Participating Media: The Past, The Present, and Some Possible Futures," *Journal of Heat Transfer*, Vol. 110, No. 4(B), 1988, pp. 1220–1229.

[2]Zhang, J. M., and Sutton, W. H., "Multidimensional Radiative Transfer in Absorbing, Emitting and Linearly Anisotropic Scattering Cylindrical Medium with Space-Dependent Properties," *Journal of Quantitative Spectroscopy and Radiative Transfer*, Vol. 52, No. 6, 1994, pp. 791–808.

[3]Fiveland, W. A., "A Discrete Ordinates Method for Predicting Radiative Heat Transfer in Axisymmetric Enclosures," American Society of Mechanical Engineers Paper 82-HT-20, 1982.

[4]Crosbie, A. L., and Schrenker, R. G., "Radiative Transfer in a Two-Dimensional Rectangular Medium Exposed to Diffuse Radiation," *Journal of Quantitative Spectroscopy and Radiative Transfer*, Vol. 31, No. 4, 1984, pp. 339–372.

[5]Menguç, M. P., and Viskanta, R., "Radiative Transfer in Axisymmetric, Finite Cylindrical Enclosures," *Journal of Heat Transfer*, Vol. 108, No. 2, 1986, pp. 271–276.

[6]Thynell, S. T., "Treatment of Radiation Heat Transfer in Absorbing, Emitting, Scattering, Two-Dimensional Cylindrical Media," *Numerical Heat Transfer-Part A*, Vol. 17, 1990, pp. 449–472.

[7]Jendoubi, S., Lee, H. S., and Kim, T., "Discrete Ordinates Solutions for Radiatively Participating Media in a Cylindrical Enclosure," *Journal of Thermophysics and Heat Transfer*, Vol. 7, No. 2, 1993, pp. 213–219.

[8]Naraghi, M. H. N., and Kassemi, M., "Analysis of Radiative Transfer in Rectangular Enclosures Using a Discrete Exchange Factor Method," *Journal of Heat Transfer*, Vol. 111, No. 4, 1989, pp. 1117–1119.

[9]Pessoa-Filho, J., and Thynell, S. T., "Development of an Approximate Solution to the Equation of Transfer in Slab and Spherical Geometries," *Journal of Quantitative Spectroscopy and Radiative Transfer*, Vol. 52, No. 1, 1994, pp. 59–73.

[10]Pessoa-Filho, J., and Thynell, S. T., "Approximate Solution to the Equation of Radiative Transfer in Cylindrical Participating Media," *Journal of Quantitative Spectroscopy and Radiative Transfer*, Vol. 53, No. 5, 1995, pp. 533–547.

[11]Özişik, M. N., *Radiative Transfer*, Wiley, New York, 1973.

[12]Dunderstadt, J. J., and Martin, W. R., *Transport Theory*, Wiley, New York, 1979.

[13]Dennar, E. A., and Sibulkin, M., "An Evaluation of the Differential Approximation for Spherically Symmetric Radiative Transfer," *Journal of Heat Transfer*, Vol. 91, Feb. 1969, pp. 73–76.

[14]Chai, J. C., Lee, H. S., and Patankar, S. V., "Ray Effect and False Scattering in Discrete Ordinates Method," *Numerical Heat Transfer-Part B*, Vol. 24, No. 4, 1993, pp. 373–389.

[15]Chai, J. C., Lee, H. S., and Patankar, S. V., "Evaluation of Spatial Differencing Practices for the Discrete-Ordinates Method," *Journal of Thermophysics and Heat Transfer*, Vol. 8, No. 1, 1994, pp. 140–144.

[16]Abramowitz, M., and Stegun, I., *Handbook of Mathematical Functions*, Dover, New York, 1964.